A concrete composite from biologically based binders and mineral aggregates for constructional 3D-printing

Christ, J.; Ottosen, L.M.; Koss, H.

Published in:
Proceedings ICSBM 2019

Publication date:
2019

Document Version
Publisher's PDF, also known as Version of record

A concrete composite from biologically based binders and mineral aggregates for constructional 3D-printing

J. Christ[1], H. Koss[1], L.M. Ottosen[1]

[1]Department of Civil Engineering, Technical University of Denmark, Brovej 118, 2400 Kgs. Lyngby

Abstract

The paper presents an alternative binder for structural 3D-printing with composite materials. The binder eases the control of setting times after extrusion through thermoplastic hardening properties. The material could therefore enable the production of thin-walled geometries in large-scale 3D-printing with higher degrees of freedom in respect to overhanging geometries without supporting structures. The proposed composite material is made from mineral aggregates and biological gels, resourced from animal tissue and bone. The used mineral aggregates are not deviating significantly from conventional concrete or mortar.

So far, the research determined a maximum flexural- and compressive strength of 8 MPa and 21 MPa. Furthermore, first material compositions are introduced and respective material properties tested. As a conclusion, the paper presents limitations and potentials of the concrete for the use as structural building material and the use within large-scale 3D-printing.

Keywords: Bio-based concrete, constructional 3D-printing, biopolymers, concrete composite, mineral aggregates

ICSBM 2019
ID 119

1. Introduction

Additive manufacturing and 3D-printing in the construction sector is a rapidly growing field of interest in research and industry [1], [2]. Possible material savings and a higher degree of freedom in shape forming increase both, sustainability in construction and architectural expression [3]. Some of the materials used for constructional three dimensional extrusion processes are steel ([4], [5]) , carbon fibre[6], or polymers ([7], [8], [9]). The main focus however lays on the printing with concrete ([1], [3], [10]), due to proven beneficial properties of cementitious materials, such as durability, inexpensiveness, fire resistance, structural strength and its plasticity during extrusion.

The current focus on cementitious concrete has its drawback regarding its sustainability account. This is due to the high amount of energy used under production, the CO_2-emissions of the chemical process during calcination of limestone and the high transport efforts due to dependency on centralised large-scale production sites. In many cases, the extruded material comprises substantially higher cementitious shares than conventionally casted concretes [11]–[13]. Additionally, extensive admixtures are being used to adapt the composite's performance as intended, enabling rapid viscosity change from liquid to solid during the printing process by thixotropic or chemical procedures. The combination of large limitations in reinforcement integration [3] and low early-age strength of concrete causes buckling and moment failures during printing, and restrain degree-of-freedom to an almost vertical build up.

The here presented research proposes an alternative concrete composite, based on biologically (bio-) based binding materials, for constructional 3D-printing. This concrete is in the following referred to as Biopolymer Concrete (BPC). The novelty of the material is the compound of biopolymers, resourced from animal tissue, bones, fish, shellfish, or algae as binding material in concrete, purposed for additive manufacturing processes. The intention is to completely replace any cementitious share in the composite with the biopolymer- and water- based binders. Sought after properties of the BPC with regards to constructional 3D-pinting are rapid viscosity change due to its thermoplastic hardening. Possibly, higher material savings in comparison to cementitious concrete could be reached by enabling higher resolution prints, i.e. thin-walled and overhanging geometries, through the rapid solidification.

Different sources for the binding material are considered. As a first prove of construction-worthiness of the novel material, the research presented here is conducted with BPC samples made of bone glue, a biologically resourced gel from animal tissue and bones (meat industrial waste products). The samples were tested for compressive- and flexural strength with different binder contents in the composite material. Other properties relating to the construction process, i.e. printability of the concrete, such as hardening and drying time as well as shrinkage, density and thermoplasticity have been tested explicitly or will be discussed based on available information.

2. Methodology

2.1 Materials

The tested BPC composite material was manufactured using bone glue as bio-based binding material, and mineral aggregates. In the following, the individual components, are described and characterized.

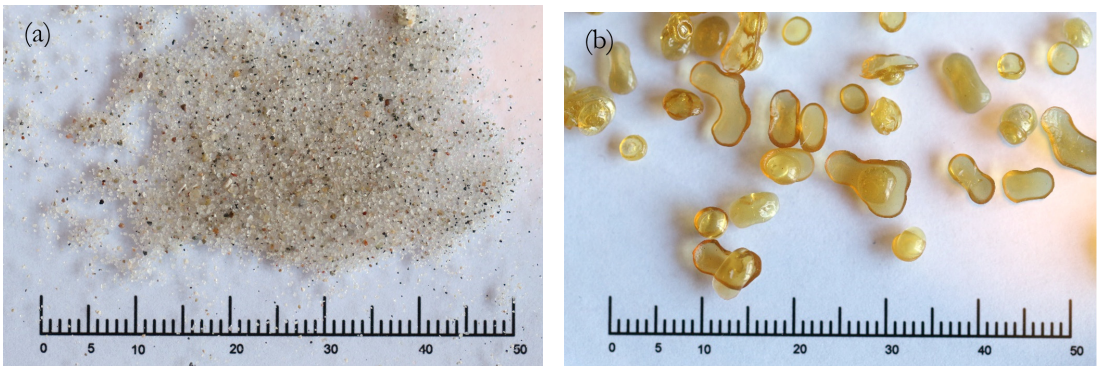

Figure 1: Raw materials used for BPC – (a) Mineral aggregates: Sand with a grain size distribution between 0-2mm, (b) biologically based binder granulate: bone glue – in [mm]

2.1.1 Mineral Aggregates

The used mineral aggregates are limited to sand with a grain size composition of 0-2mm (Figure 1 - a). The used sand is taken from the Great Belt strait in Denmark, part of the Baltic Sea. Due to the maritime origin,

The small grain size was chosen to:

reach a sufficient homogeneity of the composite material for small sample sizes

assure applicability for constructional 3D printing, for which rather small grained aggregates are used (as in [12], [13]) to enable thin extrusion processes and high resolution.

the rounded shape adds to good workability of the fresh concrete mix

2.1.2 Bio-based binding material

Bone glue is used as a biologically based binder to produce test specimen in this paper. The material is commercially available and extracted from industrial waste in food production (animal tissue and bones). It is traditionally used as adhesive for carpentry, woodwork, as well as for restauration and instrument making. Under soaking of water and the influence of heat, covalent bonds of long chained bio-polymers dissolve and a biological gel is separated from the raw biological material by Gelatinization. The adhesive is dried and sold in form of granulate (see Figure 1 – b).

The bone glue was purchased from DICTUM [14], a supplier for woodworking tools and materials. The delivered glue granulate has a grain size of 2-7mm (Figure 1 – b). Covered with water, the granulate dissolves and the gel liquefies. This process is intensified when adding heat to the solution. Both, water content and temperature in particular affect the viscosity of the gel significantly (thermoplasticity) and are hence pivotal to the workability of the composite material. The viscosity decreases significantly when increasing the binder's temperature to 70°C. The raw granulates density is $1.3 \frac{g}{cm^3}$ [1].

2.1.3 Nomenclature

To specify the composition of the tested BPC materials, a coding indicating the different constituents by letters and numbers of mass percent is used. In this study, specific constituents are water **(W)**, bone glue **(BG)** and Great Belt sea sand 0-2mm **(Z1)**. Symbols for less specified groups or more general terms would be glue granulate **(GG)** or binder **(b)**. This system allows to write unspecific (1) and specified (2) balanced equations describing BPC materials:

$$b1 = 44GG + 56W \tag{1}$$

$$BPC1 = 10(44BG56W)90Z1 \tag{2}$$

Equation (2) omits arithmetic operators (+) as used in equation (1). The unspecified glue granulate in equation (1) is in equation (2) replaced with the specific reference to bone glue. In this way, the notation allows defining parent types and sub groups of binders and composites. Finally, a specific sample of any BPC material is identified by a unique number at the end of the material code separated by a dot. The fifth sample made of BPC1 would bear the code:

$$BPC1.5 = 10(44BG56W)90Z1.5 \tag{3}$$

All numeric values and ratios refer to the material's weight and to compositions under mixing. The specified material proportions do not account for hardened samples, since water content decreases during drying.

2.1.4 Mixture

The tested compositions consist of bone glue, water and mineral aggregates. The specifications of the different BPC materials are listed in Table 1. In all cases, a W/GG-ratio of 1.25 has been chosen due to benefits in the workability of the heated mass. This was found during preliminary experiments. Material coding is according to Section 2.1.3.

2.2 Methods

The used methods for mixing, moulding and testing are largely inspired by the standardised procedures for cementitious mortar and concrete as described in EN 196-1 [15]. However, due to thermoplastic properties of the binding material, some adaptions were made. The steps in sample production, testing and property

1 Characterised by weight and volumetric analysis with water bath. A weight scale with an accuracy of 0.01g was used, as well as a single graduated 100ml cylinder to measure the volumetric increase of 50ml of water by adding 20g of binder granulate.

ICSBM 2019
ID 119

characterisation are in the following described in more detail.

2.2.1 Composite production

The production of the concrete composite, including the process for moulding and drying is compiled in Table 2, with approximate durations of the individual steps.

Table 1: Overview of the used material compositions.

#	Sample	Binder-content	Glue granulate-content	Water-content	Aggregate-content
[-]	[-]	[wt.%]	[wt.%]	[wt.%]	[wt.%]
BPC1	10(44BG56W)90Z	10	4.44	5.56	90
BPC2	15(44BG56W)85Z	15	6.67	8.33	85
BPC3	20(44BG56W)80Z	20	8.89	11.11	80
BPC4	25(44BG56W)75Z	25	11.11	13.89	75

Table 2: In-sum process specifications for the production of bio-based concrete composite samples.

Process #	Process specification	Duration	Notes
1	Soaking of GG in W	>1h	Soaking of glue granulate in water
2	Heating	~1h	Heating of Z and b in oven to 70°C
3	Mixing	2min	Mixing in mortar blender, standardised in EN196-1 [15]
4	Moulding	3min	Moulded on vibration table until solidity is reached
5	Thermoplastic hardening	1 day	1 day left in mould - actual thermoplastic hardening time substantially lower - dependant on geometry, ambient temperature, etc.
6	Demoulding		Demoulding 1day after casting
7	Dry-hardening A	1 day	Dry hardening under room temperature
8	Dry-hardening B	4-48 days	Dry hardening in well ventilated oven at 50°C

1. Soaking of GG in W: Soaking the glue granulate in water for >1 hour, until a homogenous concentration of gel in the GG-W mix could be reached. The granulate increases its volume in reaction with water. The viscosity in this step depends on both, amount of added water and soaking time, and can range from solid to liquid. Frequently, the mix has been stirred with a glass spatula.

2. Heating of constituents: The viscosity of the GG-W mix can be decreased by heating (thermoplasticity). The water addition can be thereby decreased due to temperature control. To avoid sudden cooling and undesired hardening during the mixing process of the binder, aggregates are heated as well. Both materials are heated to 70°C to ensure the plasticity of the mix. Higher temperatures were avoided to prevent damage of the molecular structure.

Mixing of constituents: The heated constituents are mixed with a mortar blender for conventional cementitious material (Mixer specification: Seger – Tonindurtie), standardised in EN196-1 [15]. The mixing vessel is prior tempered to 70°C to prevent premature cooling of the mass. A homogenous material mix could be assumed after 2 minutes of mixing. The mixing and moulding was conducted at room temperature, giving a time limitation for the mixing. Due to cooling, the mass becomes unworkable after a short time (about 5-10min).

Moulding: The composite material is poured into moulds. This is done in a rather rapid fashion to prevent the material from premature stiffening. The moulds were filled on a vibration table to prevent large captivities and larger inhomogeneity inside the sample. The vibration was conducted with 60-80Hz until the material

increased in viscosity (approx. 3min). Prism moulds with dimensions of 40x40x160mm (width/height/length) after EN 196-1 [15], as well as cylinders with a measurement of 50x100mm (diameter/height) were used. Metal surfaces of the moulds needed to be covered with a thin PE-foil to prevent the corrosion caused by the acidic nature of the bio-binder.

1. Thermoplastic hardening: Thermoplastic hardening occurs directly after the binding material is removed from a heat source and placed in a cooler ambient temperature. The material's viscosity increases noticeably throughout mixing and moulding process.

2. Demoulding of the samples was conducted one day after moulding, to support the integrity of the sample by reaching additional strength through the outset of the dry hardening process.

3. Dry hardening: Even if the material shows stiffness after the thermoplastic hardening process, the material still contains water which prevents the biopolymers to form stronger bonds. After all water is evaporated, the material is considered as hardened. The duration of this process is dependent on water content, dimension of the sample, aggregate content and porosity. To accelerate the process for testing, samples were, after one day drying under room temperature, placed in a well ventilated oven (Oven specification: Memmert UF 160) at 50°C. For most samples, an oven drying time of 21 days was chosen.

2.2.2 Structural testing of cylindrical samples

A total of 12 cylindrical samples, 50mm diameter and 100mm height, were casted to determine compressive strengths. For loading tests, an 'Instron-6025' with a capacity of 100kN was used to load the samples, as well as for recording of force and displacement. Circular platens with a diameter of 50mm were used to slender the apparatus' loading surface down to the geometry of the material cylinders. Force was applied with a loading rate of 2400 N/s.

The moulding and drying of the samples left the top and bottom surfaces of the cylinders uneven. The samples were cut with a circular saw to a length of ~90mm before testing and after drying. The sawing was conducted slowly and without any water-cooling of the blade to prevent the material from weakening by water soaking.

2.2.3 Structural testing of prism samples

Prism samples with the size of 40x40x160mm were tested for flexural- and compressive strength according to EN196-1 [15].

For flexural strength, the prism samples were tested in a three-point bending test as standardized with a distance of the supporting rollers of 100mm and a loading rate of 50N/s on an 'Instron-6022' with a loading capacity of 10kN. The specimen was mounted with the from the moulding created even surfaces in contact with the flexure device.

The compressive strength was measured for each of the two fragments obtained from the segmentation when measuring the flexural strength. Above and below, the specimen was loaded on a surface of 40x40mm. The orientation of the samples for compressive strength was in accordance to the flexural tests, described above. Loading was applied at a rate of 2400N/s with an 'Instron-6025' testing machine with a loading capacity of 100kN.

2.2.4 Density-measurements of the composite

Calculated as ratio of individually measured mass (accuracy 0.01g) and volume (accuracy 0.01mm).

2.2.5 Shrinkage

Shrinkages of prism samples were determined by evaluating the differences in length before and after dry hardening, i.e. immediately after demoulding and before testing. Therefore, shrinkage information relates only to the dry-hardening process during this time and not to thermoplastic-hardening.

2.2.6 Dry-hardening times

The binding material develops strength over the thermoplastic- and the dry-hardening period. The duration of the thermoplastic hardening was short and easy controllable by temperature. The duration of the dry-hardening depends on geometry, porosity, ambient temperature and binder or water contents. A total of 12 cylindrical samples of BPC3 have been tested in compression (see Section 2.2.1 and 2.2.2) to evaluate the rapidity of the drying process. The sample production was conducted as indicated in Table 2. The duration of step 8 was varied. Three samples have been tested, respectively after 4, 12, 22 and 48 days of oven drying at 50°C. To keep samples comparable, the W/GG and b-content has not been varied and kept on 1.25 and 20%.

3. Results and discussion

3.1 Results

Examples of BPC are seen in Figure 2.

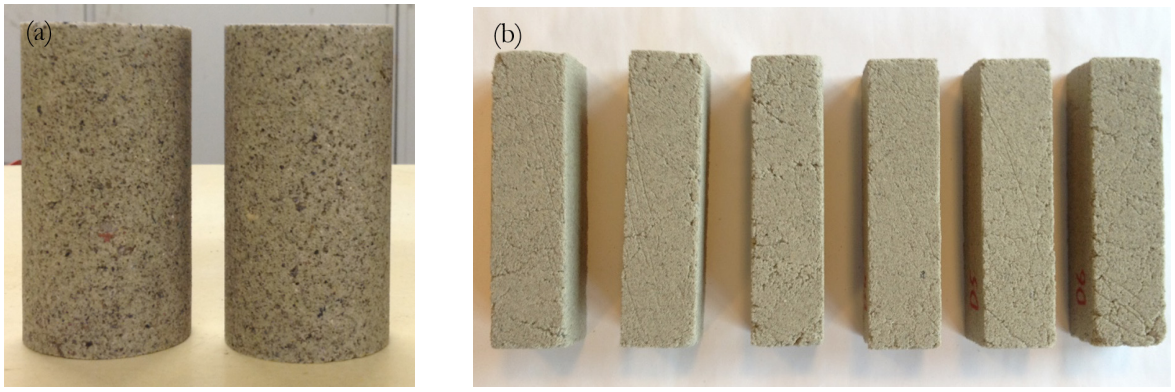

Figure 2: Biopolymer Concrete (BPC) Samples: (a) circular cylinders 100mm high and 50mm in diameter, (b) square prism samples with a length of 160mm and a cross-section of 40x40mm.

3.1.1 Property variations under hardening

The two hardening characteristics, thermoplastic- and dry-hardening, are key-influencer on the materials strength and viscosity. The thermoplastic hardening time already occurs after several minutes after discontinuity of heat exposure, the material's viscosity increases and the composite gains integrity. Due to the obvious relation of the material's temperature to its fluidity, the rapidity of the process is thought to be connected with the composite's geometry, heat capacity, water content, initial- and ambient temperature. The observations of this process proposes therefore, its simple controllability. The subsequent dry hardening can be described as the water loss through evaporation and extends, dependant on the water content, over a longer period of time.

Figure 3 shows the dependency of the compressive strengths on this dry-hardening duration. Illustrated results display that the material strength is increasing for an increase of dry-hardening time, suggesting that the strength of the material is strongly dependant on its water content. Hence, a high water content implies low strength and an advanced drying process a higher strength. The four data points were tested with a respective sample quantity of three, namely samples BPC3.1-12 (Figure 2 – a). The mean of each tested

point in time has been connected by a smoothened line. A substantial increase of compressive strength was observed (until 22 days), where after the graph flattens. The flattening starts between 12 days and 22 days, an exact point in time, however, could not be determined. For the values around the flattening, the graph shows larger variabilities. Contrary, minor variations were observed for short and extensive dry-hardening durations. A bend in the smoothened curve of Figure 3 denotes a characteristic change of drying rapidity.

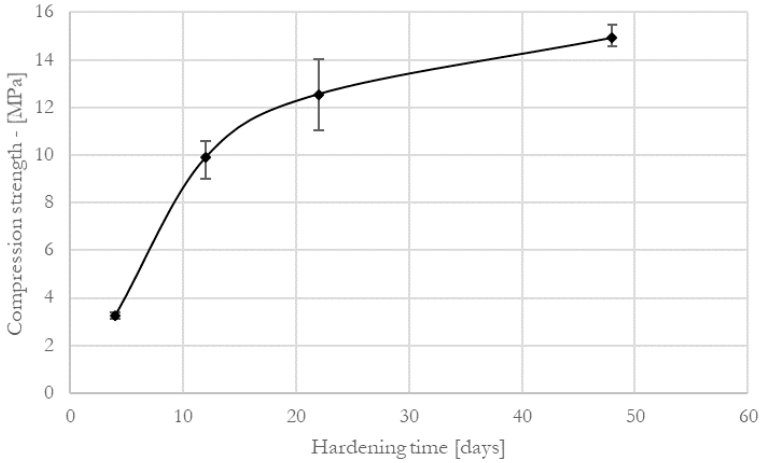

Figure 3: Compressive strength of cylindrical samples BPC3.1-12. over dry hardening times at 50°C (corresponding to step 8 in Table 2). The error bars show maximum and minimum values. The connecting line has been smoothened.

The drying characteristics are expected to be geometry dependent, as well as reliant on initial water content, ambient temperature and humidity. Other than the thermoplastic hardening, dry hardening is expected to not conclude, but rather to approximate asymptotically to an upper bound, which is dependent on the ambient humidity. Therefore, varying water contents through differing binder to aggregate compositions, possibly show divergent hardening times. This, however is up to date not experimentally verified.

3.1.2 Density

Characterizing density and shrinkage is useful to evaluate the material on its suitability for constructional 3D printing by limiting self-weight and shrinkage cracking. For sample batches BPC1, BPC2, BPC3, and BPC4 (cf. Table 1); volume, weight and length have been measured before testing and after drying. Respectively calculated density values can be seen in Figure 4. The mean values range from 1.6g/cm^3 to 1.4g/cm^3 for varying binder contents. Densities generally decrease with a decrease in aggregate shares in the mix.

The material's density is scattered around a value of about 1.5 g/cm^3. The composite is therefore lighter than cementitious mortar, which is here assumed with the typical value of 2.2 g/cm^3. The mixing ratios influences the material's density only marginally for a binder content of 10%-20% (BPC1, BPC2, BPC3). A content of 25%, however, causes a large density loss of 10%. Due to the comparably high density of the used sand (2.6 g/cm^3), low density binder (1.3 g/cm^3), and the continuous change of mixing ratios (10%, 15%, 20%, 25% binder content) throughout the tests, a linear decrease of density could have been expected. Contrary, the non-linear appearing measurements of Figure 4 let suppose, that the pore content for samples with a binder content of over 20% increases substantially, i.e. its density decreases.

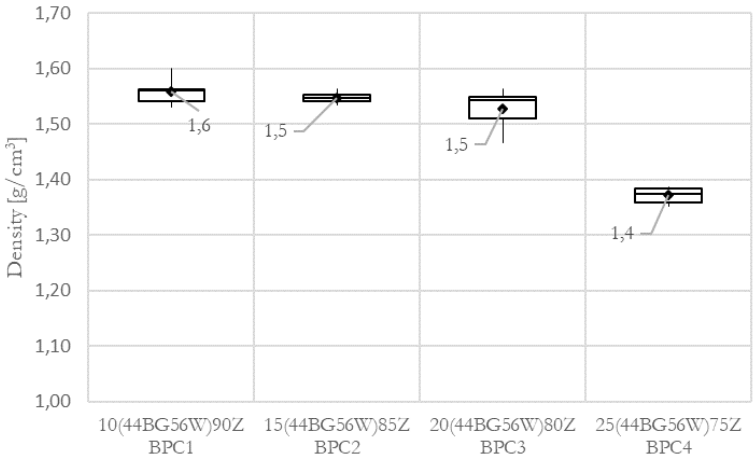

Figure 4: Density of sample batches with varying binder contents. Whiskers show maximum and minimum value of the data set; boxes define upper, middle and lower quartile; the marker shows mean values. Each boxplot is substantiated with a data point quantity of six measurements.

3.1.3 Shrinkage

The densities tendency is reversely reflected by shrinkage ratios in Figure 5. The continuous increase of the data set ranges from 0.3% to 2% and increases for higher binder contents. Therefore, shrinkage appears to be directly interlinked to the materials composition, or rather to the binder's water content. The results suggest that the evaporation of water causes the material to shrink.

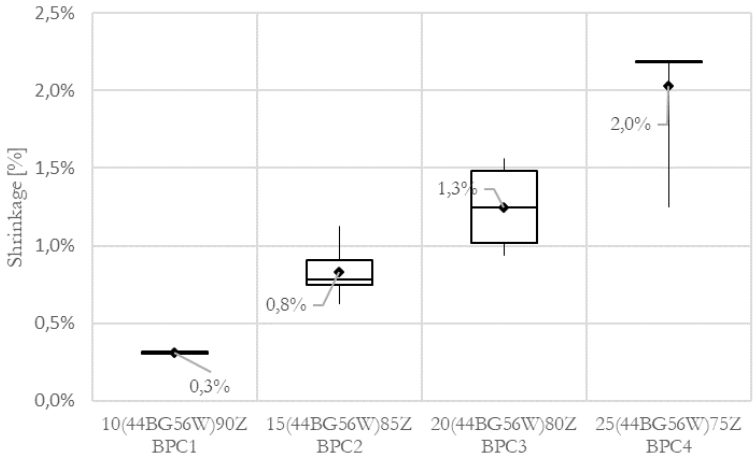

Figure 5: Shrinkage of sample batches with varying binder contents. Whiskers show maximum and minimum value of the data set; boxes define upper, middle and lower quartile; the markers show mean values. Each boxplot is substantiated with a data point quantity of six measurements.

3.1.4 Strength of BPC

The composite's properties are expected to be strongly dependant on the material's composition. Therefore, the dependencies on varying binder-contents were measured to determine performance peaks of flexural and compressive strength. Six prisms (Figure 2-b) for each composition were casted with a binder content of 10%, 15%, 20% and 25% (BPC1-4) and a W/GG-ratio by weight of 1.25. Corresponding mixtures can be found in Table 1, a dry-hardening duration of 21 days was chosen for all samples. Figure 6 and 7 show the obtained results for flexural and compressive strengths.

Flexural strength: As shown in Figure 6, batch BPC2 had the highest flexural strength, i.e. the batch with a binder content of 15%. When lowering the binder content to 10% (Batch BPC1), the flexural strength

was more than halved. Increasing the binder content to 20% and 25%, i.e. BPC3 and BPC4, resulted in a decreased flexural strength, though not as significant as for the prisms with 10% binder.

Compressive Strength: The compressive strength for the prisms are shown in Figure 7. A tendency to a maximum mean compressive strength of batch BPC3 can be identified as a peak performance value. However, the upper error bar for batch BPC3 has a relatively large magnitude and is decisive for an increased mean value, being higher than middle and upper quartile. Therefore, a difference between batch BPC2 and BPC3 can not be concluded. A major drop in strength is located between BPC3 and BPC4.

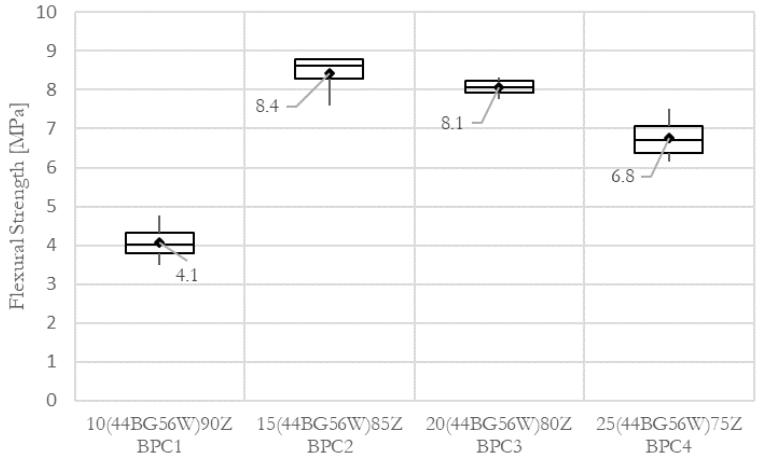

Figure 6: Flexural strength of prism samples with varying binder contents. Whiskers show maximum and minimum value of the data set; boxes define upper, middle and lower quartile; the marker shows mean values.

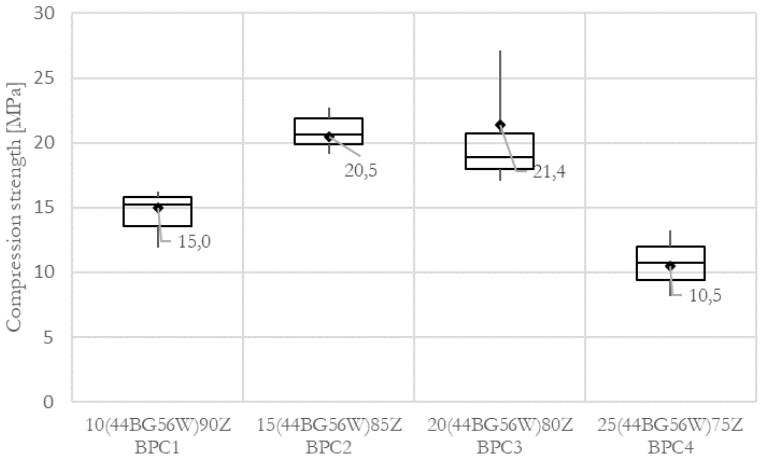

Figure 7: Compressive strength testing of prism samples with varying binder contents. Whiskers show maximum and minimum value of the data set; boxes define upper, middle and lower quartile; markers show mean values.

Both, flexural and compressive strength suggest a performance peak between 15% and 20% binder content. The peaking of strength in this range, and the subsequent decrease for higher binder contents can potentially be explained with: 1) an increase of porosity due to the higher binder content and therefore decrease in density and strength (see Figure 4), or 2) an incomplete or not comparable dry-hardening process between varying binder contents as described in Section 3.1.1.

Even though in similar range, flexural- and compressive strength propose diverging mean performance peaks in the margin of 15%-20%. The boxplots however do show similar order for both stresses in Figure 6 and 7. The correlation of mean flexural- and compressive strength was therefore evaluated to determine

the consequences of an increase of binder content in the mixture. The results are shown in Figure 8. It appears that the two properties react differently on the composition change. A consistent ratio in strength could therefore be excluded. A general observed trend is that higher binder contents cause an increase in relative flexural strength. Contrary, low binder contents lay the performance's focus on the compressive strength. The maximum ratio in Figure 8 has a magnitude of 65% for a binder content of 25% (BPC4). The indicated performance peaks for BPC2 and BPC3 show a strength ratio of around 40%. In all cases, the ratio of flexural- to compressive strength surpasses the performance of conventional cementitious concrete, which is around 10%, as a rule of thumb.

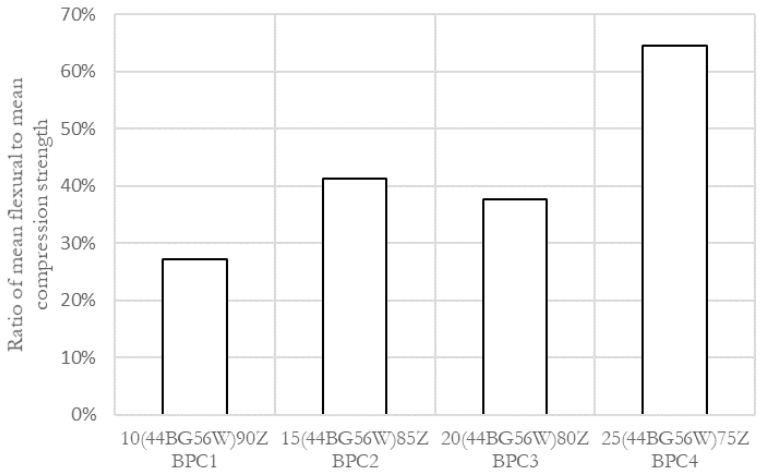

Figure 8: Ratio of flexural strength to compressive strength for varying binder contents. Mean values of measured strengths as in Figure 6 and 7 were used.

3.2 Discussion

The BPC's properties were tested to assess the materials suitability for constructional 3D-printing. In the following, the results are brought into context, i.e. 'suitable'- and 'to be further advanced' properties are listed and compared.

Suitable properties of BPC for constructional 3D-printing:

Printability of BPC: Primary advantage of BPC for constructional 3D-printing is the easy controllable thermoplastic hardening and thickening of the material. The in Section 2.2 and 3.1.1 discussed thermoplasticity shows, that the material increases rapidly in viscosity only by the exposure to room temperature. During an envisaged printing process, the material itself would therefore not only rely on the thixotropic build-up of the composite material, as for 3D-printing with cementitious concrete [16]. By the ability of controlling the thermoplasticity to a high degree, and increasing the early age strength of the matrix, the thinness of layers could be increased and potential early age moment failure of the built up prevented. More slender constructions and higher degree of freedom in terms of overhanging prints, could possibly be realised. This is also supported by the material's low density and high relative flexural strength, as described in Section 3.1.4, which can increase the early age moment resistance and lower the dead load added to the system under construction.

Composite strength: As proposed in Section 3.1.4, BPC shows generally a strength in the order of magnitude of cementitious concrete, though not comparable with high performance printing concretes [12]. One of the biggest challenges of constructional 3D-printing is the integration of reinforcement [3]. The printing process prevents the placing of extensive steel reinforcement and limits the freedom of shape

for cementitious concrete substantially due to the lack of flexural strength in cementitious materials. With a high ratio of flexural- to compressive strength of BPC, as described in Section 3.1.4, the BPC material could deliver a filament that could render building components loaded in flexure and thereby diminish the need for reinforcement.

Structural integrity of prints: Assuming a layer-by-layer 3D-printing process for the constructional use of the material, the integrity of the meso-scale structure is at risk by possibly exceeded shrinkage limits or detachment of layers through lacking interface adhesion [17]. Shrinkage, as evaluated in Section 3.1.3, can be controlled by editing the binder content. Possibly, fibre reinforcement could be added to limit shrinkage cracking. The found shrinkage ratios of 0.3% to 2% is therefore evaluated as suitable for constructional 3D-printing. The bone glue has furthermore been traditionally used for carpentry constructions and instrument making and adheres well to itself. It is therefore expected, that the contact surface of a printed layer bonds well to precedent layers. This, however needs to be experimentally verified in further work.

- *Sustainability:* The substitution of high cement contents and extensive admixtures in constructional 3D-printing filaments with biologically based binders such as bone glue could have a positive impact on the sustainability account of the method. This is due to lower production temperatures of bone glue in comparison to cement, and avoidance of CO_2-emissions under the calcination of limestone.

BPC properties, crucial to be further advanced:

- *Durability:* BPC has, due to its organic compounds and hygroscopic behaviour, a high risk of fast deterioration. During the testing, some of the samples, especially for binder contents over 20%, showed moulding attack.
- *Fire resistance:* The thermoplastic properties of the material are expected to be beneficial for the 3D-printing process but disadvantageous for its fire-resistance. The fireproofing of the material is crucial for further development.
- *Hygroscopic properties:* As described in Section 3.1.1, the water content is decisive for the structural strength of the material. Removing the water contents, hardens the material. The process can also be reversed, i.e. exposure of the hardened material to water softens its strength, which is critical for the use as structural material.

An overview of the above described can be found in Table 4.

Table 4: In sum – advantageous properties in comparison to ongoing advancements

Properties of BPC, suitable for constructional 3D-printing	Properties of BPC, crucial to be advanced
Thermoplasticity	Durability
Flexural- /compressive strength	Fire resistance
Low density	Water resistance
Self-adhesion	
Shrinkage	

4. Conclusions

A composite of a biopolymer binding material (bone glue – a bio-gel produced from the meat industry's waste) in conjunction with mineral aggregates was evaluated on its suitability as a filament for constructional 3D-printing of concrete. The findings show structural strengths in the order of magnitude of conventional concrete, i.e. flexural strength of 8 MPa and compressive strength of 21 MPa, and suggest therefore the

composite's usability as a structural building material. A density of around 1.5 g/cm^3, easy controllable thermoplastic hardening characteristics, and a high moment resistance through high flexural- to compressive strength ratios of up to 65%, propose furthermore the benefit for additive manufacturing processes. Low induced dead loads, early-age material strength and high moment resistance, could diminish the need for reinforcement integration of 3D-printed structures, and enable higher degrees of freedom in terms of overhanging and thin geometries. The results suggest the suitability of bone glue as a binding material for concrete and the use in constructional 3D printing, linked with further research and development work for the composite's durability, fire- and water resistance.

5. Acknowledgment

The presented research work in this paper has been financed by Ingeniør Kaptajn Aage Nielsens Familiefond, grant (00023307) from VILLUM FONDEN (VILLUM Experiment), and DTU's Department for Civil Engineering. We thank our lab-personnel for technical advice and assistance.

6. References

[1] Y. W. D. Tay, B. Panda, S. C. Paul, N. A. Noor Mohamed, M. J. Tan, and K. F. Leong, "3D printing trends in building and construction industry: a review," *Virtual Phys. Prototyp.*, vol. 12, no. 3, pp. 261–276, 2017.

[2] N. Labonnote, A. Rønnquist, B. Manum, and P. Rüther, "Additive construction: State-of-the-art, challenges and opportunities," *Autom. Constr.*, vol. 72, pp. 347–366, 2016.

[3] F. Bos, R. Wolfs, Z. Ahmed, and T. Salet, "Additive manufacturing of concrete in construction: potentials and challenges of 3D concrete printing," *Virtual Phys. Prototyp.*, vol. 11, no. 3, pp. 209–225, 2016.

[4] S. Ren and S. Galjaard, "Topology Optimisation for Steel Structural Design with Additive Manufacturing Shibo," in *Modelling Behavior*, 2015, pp. 35–36.

[5] "MX3D Bridge." [Online]. Available: https://mx3d.com/projects/bridge-2/. [Accessed: 26-Apr-2019].

[6] A. Menges, "BUGA Fibre Pavilion 2019 | Institute for Computational Design and Construction," 2018. [Online]. Available: https://icd.uni-stuttgart.de/?p=22271. [Accessed: 26-Apr-2019].

[7] S. J. Keating, J. C. Leland, L. Cai, and N. Oxman, "Toward site-specific and self-sufficient robotic fabrication on architectural scales," *Sci. Robot.*, vol. 2, no. 5, 2017.

[8] G. Pasquarelli, W. Sharples, C. Sharples, and R. Caillouet, "Additive Manufacturing Revolutionizes Lightweight Gridshells," 2017.

[9] L. Mogas-Soldevila and N. Oxman, "Water-based engineering & fabrication: Large-scale additive manufacturing of biomaterials," *Mater. Res. Soc. Symp. Proc.*, vol. 1800, pp. 46–53, 2015.

[10] I. Perkins and M. Skitmore, "Three-dimensional printing in the construction industry: A review," *Int. J. Constr. Manag.*, vol. 15, no. 1, pp. 1–9, 2015.

[11] D. Marchon, S. Kawashima, H. Bessaies-Bey, S. Mantellato, and S. Ng, "Hydration and rheology control of concrete for digital fabrication: Potential admixtures and cement chemistry," *Cem. Concr. Res.*, vol. 112, no. December 2017, pp. 96–110, 2018.

[12] T. T. Le, S. A. Austin, S. Lim, R. A. Buswell, A. G. F. Gibb, and T. Thorpe, "Mix design and fresh properties for high-performance printing concrete," *Mater. Struct. Constr.*, vol. 45, no. 8, pp. 1221–1232,

2012.

[13] Y. Zhang, Y. Zhang, W. She, L. Yang, G. Liu, and Y. Yang, "Rheological and harden properties of the high-thixotropy 3D printing concrete," *Constr. Build. Mater.*, vol. 201, pp. 278–285, 2019.

[14] "More than Tools | Dictum." [Online]. Available: https://www.dictum.com/en/. [Accessed: 23-Apr-2019].

[15] DS/En 196-1, "Metoder til prøvning af cement – Del 1: Styrkebestemmelse Methods of testing cement – Part 1: Determination of strength," 2016.

[16] R. J. M. Wolfs, F. P. Bos, and T. A. M. Salet, "Early age mechanical behaviour of 3D printed concrete: Numerical modelling and experimental testing," *Cem. Concr. Res.*, vol. 106, no. May 2017, pp. 103–116, 2018.

[17] Y. W. D. Tay, G. H. A. Ting, Y. Qian, B. Panda, L. He, and M. J. Tan, "Time gap effect on bond strength of 3D-printed concrete," *Virtual Phys. Prototyp.*, vol. 14, no. 1, pp. 104–113, 2019.